

**$K^*\Sigma$  photoproduction off the proton target with baryon resonances**Sang-Ho Kim,<sup>1,2,\*</sup> Seung-il Nam,<sup>3,†</sup> Atsushi Hosaka,<sup>1,‡</sup> and Hyun-Chul Kim<sup>2,§</sup><sup>1</sup>*Research Center for Nuclear Physics (RCNP), Osaka 567-0047, Japan*<sup>2</sup>*Department of Physics, Inha University, Incheon 402-751, Republic of Korea*<sup>3</sup>*School of Physics, Korea Institute for Advanced Study (KIAS), Seoul 130-722, Republic of Korea*  
(Dated: November 28, 2012)

We investigate the photoproduction of  $K^{*0}\Sigma^+$  and  $K^{*+}\Sigma^0$  off the proton target, employing the effective Lagrangian approach at the tree-level Born approximation. In addition to the  $(s, t, u)$ -channel Born diagrams, we take into account various baryon-resonance contributions such as  $F_{15}(2000)$ ,  $D_{13}(2080)$ ,  $G_{17}(2190)$ ,  $D_{15}(2200)$ ,  $F_{35}(2000)$ ,  $G_{37}(2200)$ ,  $F_{37}(2390)$ , and  $\Sigma^*(1385, 3/2^+)$  in a fully covariant manner. We present the numerical results for the energy and angular dependences for the cross sections in comparison to available experimental data. The single-polarization observables, i.e. the photon-beam ( $\Sigma_\gamma$ ), recoil ( $P_y$ ) and target ( $T_y$ ) baryon polarization asymmetries are computed as well for future experiments. We observe from the numerical results that the resonance contributions play a minor role in producing the strength of the cross sections, being different from the  $K^*\Lambda$  photoproduction. In contrast, it turns out that the  $\Delta(1232)$ -pole contribution and strange-meson exchanges in the  $t$ -channel dominate the scattering process. On the other hand, the higher resonances influence the polarization observables such as the recoil and target asymmetries.

PACS numbers: 13.60.Rj, 13.60.Le, 13.60.-r, 11.10.Ef, 14.20.Gk.

Keywords:  $K^*\Sigma$  photoproduction, effective Lagrangian method, baryon resonances, single-polarization observables.

\* E-mail: shkim@rcnp.osaka-u.ac.jp

† E-mail: sinam@kias.re.kr

‡ E-mail: hosaka@rcnp.osaka-u.ac.jp

§ E-mail: hchkim@inha.ac.kr

## I. INTRODUCTION

Strangeness production via various scattering processes has been one of the most important issues in hadronic and nuclear physics for decades. From them, we can understand the microscopic mechanism of the productions beyond the light-flavor sectors and extend our knowledge into multi-strangeness states. In this sense, photoproduction of strange hadrons off the nucleon target is a very useful tool and has been widely studied experimentally as well as theoretically. For example, experiments for the photoproduction of  $\gamma N \rightarrow K\Lambda$  and  $K\Sigma$  were reported in Refs. [1–3]. Related theoretical studies were also performed in Refs. [4–7]. In particular, Ref. [4] emphasized the baryon resonance contributions, which play important roles in reproducing the experimental data. The effects of the electromagnetic form factor [5] were also investigated for the photo- and electro-production of the kaon, the Ward-Takahashi (WT) identity being explained. It was also pointed out that the tensor-meson exchange in the  $t$ -channel provides a significant contribution to kaon photoproduction [6]. An unbiased model selection, based on Bayesian inference, was introduced for extracting physical information from kaon photoproduction [7]. References [8, 9] examined the  $t$ -channel Regge trajectories to enhance the model applicabilities to actual problems.

Photoproduction of the vector strange meson ( $K^*$ ) provides even richer physics in comparison with the  $KY$  channel. For instance, Since it is a vector meson with quantum number  $I(J^P) = 1/2(1^-)$ , the exchange of the strange scalar meson  $\kappa$  is allowed in the  $t$ -channel, which is absent in the  $KY$  channel, in addition to the  $(K, K^*)$  exchanges. Moreover, the polarization of  $K^*$  in the final state is also a good physical subject to be investigated together with other polarization observable in terms of the spin-density matrices. Experimentally, this production channel has been investigated for  $\gamma N \rightarrow K^*\Lambda(1116)$  by the CLAS collaboration at Jefferson laboratory [10, 11], and  $\gamma N \rightarrow K^*\Sigma(1193)$  by the TAPS collaboration at Electron Stretcher and Accelerator (ELSA) [12], the CLAS at Jefferson laboratory [13, 14], and the LEPS at Super Photon Ring-8 GeV (SPring-8) [15]. These two processes have been extensively studied theoretically within the effective Lagrangian approaches [16–19] as well as in the chiral quark model [20]. As mentioned above, it was argued that the  $\kappa$ -exchange should play an important role in the production mechanism of  $\gamma p \rightarrow K^*\Sigma$  [17]. Interestingly enough, the recent LEPS experiment reported the experimental data that supported the importance of the scalar-meson exchange indeed [15]. Moreover, employing the same theoretical framework, Ref. [19] showed that the nucleon-resonance contributions were very crucial to reproduce the experimental data of  $\gamma p \rightarrow K^{*+}\Lambda$ .

Considering all these successful and meaningful theoretical results accumulated so far within the effective Lagrangian method with the resonance contributions taken into account, we want to explore carefully the reaction processes  $\gamma p \rightarrow K^{*0}\Sigma^+$  and  $\gamma p \rightarrow K^{*+}\Sigma^0$  in the present work. Although the  $K^*\Sigma$  photoproduction was already studied theoretically within the similar framework in Ref. [17], we will include various baryon-resonance contributions which were proven to be essential in the  $K^*\Lambda$  channel [19]. Thus, we introduce the baryon resonances as follows:  $F_{15}(2000)$ ,  $D_{13}(2080)$ ,  $G_{17}(2190)$ ,  $D_{15}(2200)$ ,  $F_{35}(2000)$ ,  $G_{37}(2200)$ ,  $F_{37}(2390)$  in the  $s$ -channel and  $\Sigma^*(1385)$  in the  $u$ -channel, in addition to the  $s$ -channel with  $N(940)$ - and  $\Delta(1232)$ -pole contributions, the  $t$ -channel with  $\kappa$ -,  $K$ -, and  $K^*$ -exchange contributions, and the  $u$ -channel with  $\Lambda(1116)$ - and  $\Sigma(1193)$ -pole contributions. These resonance contributions have not been taken into account in the previous theoretical work [17] and will be treated in a fully relativistic manner in the present work, as done for the  $\gamma p \rightarrow K^{*+}\Lambda$  [19].

The coupling strengths for strong and electromagnetic (EM) vertices are computed by using experimental and theoretical information [21–25]. As for the coupling constants for the nucleon resonances, we employ the SU(6) quark-model estimation for the strong vertices [24, 25]. In order to preserve the WT identity, we employ the gauge-invariant form factor prescription given in Refs. [26–28]. The cut-off parameters for the form factors are determined in such a way that the experimental data are reproduced. With these parameters fixed, we provide the total ( $\sigma$ ) and differential cross sections ( $d\sigma/d\Omega$ ) for the two reaction channels. In addition, the single polarization observables such as those for the photon-beam ( $\Sigma$ ), target ( $T_y$ ), recoil baryon ( $P_y$ ), are presented for useful theoretical guides for available and future experiments. Based on the present results, we observe that the resonance contributions play a minor role in producing the strength of the cross sections, being different from the  $K^*\Lambda$  photoproduction. On the other hand, it turns out that the  $\Delta(1232)$ -pole diagram and strange-meson exchanges in the  $t$ -channel play dominant roles in explaining the production mechanism of  $K^*\Sigma$ .

The present work is organized as follows: In Section II, we explain the present theoretical framework in detail and show how to determine various model parameters. The numerical results are presented and discussed in Section III. The last Section is devoted to the summary, conclusion, and future perspectives.

## II. FORMALISM

In the present work, we employ the effective Lagrangian method at the tree-level Born approximation. The relevant and generic Feynman diagrams for the reaction processes  $\gamma p \rightarrow K^{*0}\Sigma^+$  and  $\gamma p \rightarrow K^{*+}\Sigma^0$  are shown in Fig. 1, which

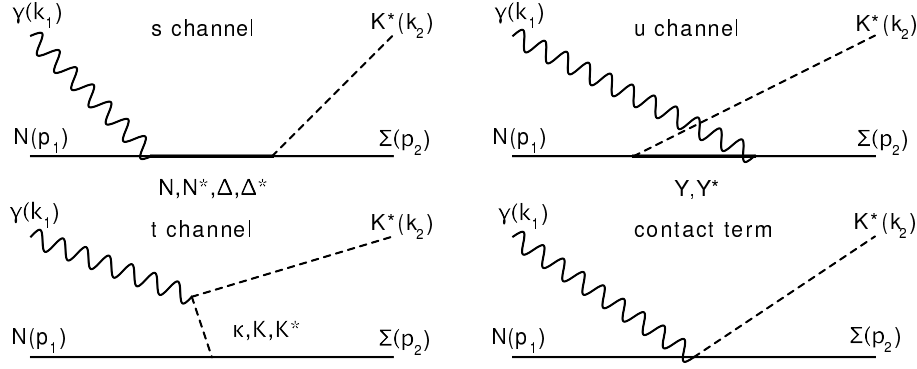


FIG. 1. Relevant Feynman diagrams for the  $\gamma N \rightarrow K^* \Sigma$  reaction process.  $N$ ,  $N^*$ ,  $\Delta$ ,  $\Delta^*$ ,  $Y$ , and  $Y^*$  denote the nucleon, nucleon resonances, delta, delta resonances, hyperons, and hyperon resonances, whereas  $\kappa$ ,  $K$ , and  $K^*$  stand for the strange scalar, pseudoscalar, and vector mesons, respectively. The four momenta for the initial and final particles are also defined as shown in the diagrams.

include  $N$ ,  $\Delta$ ,  $N^*$ , and  $\Delta^*$  poles in the  $s$ -channel, the  $K^*$ ,  $K$ , and  $\kappa$  meson exchanges in the  $t$ -channel, and  $\Lambda$ ,  $\Sigma$ , and  $\Sigma^*(1385, 3/2^+)$  hyperons in the  $u$ -channel. The contact-term contribution is necessary to satisfy the WT identity in general. For convenience, we assign these two production processes as the  $K^{*0}\Sigma^+$  and  $K^{*+}\Sigma^0$  channels, respectively, hereafter. Note that, however, we do not have the  $K^*$ -exchange for the  $K^{*0}\Sigma^+$  channel due to their electrically neutral vertex of  $\gamma K^* \bar{K}^*$  as far as we ignore the magnetic and quadratic moment of  $K^*$  as in the present work. Consequently, the contact term is also absent for the  $K^{*0}\Sigma^+$  channel.

The effective Lagrangians for the Born contributions are essentially the same as those used in Refs. [16, 19]. As for the photon-meson-meson Yukawa interactions, we define them as follows:

$$\begin{aligned}\mathcal{L}_{\gamma K^* K^*} &= -ie_{K^*} A^\mu (K_{\mu\nu}^{*\dagger} K^{*\nu} - K_{\mu\nu}^* K^{*\dagger\nu}), \\ \mathcal{L}_{\gamma K^* K} &= g_{\gamma K^* K} \varepsilon^{\mu\nu\alpha\beta} (\partial_\mu A_\nu) (\partial_\alpha K_\beta^*) K + \text{h.c.}, \\ \mathcal{L}_{\gamma K^* \kappa} &= g_{\gamma K^* \kappa} A^{\mu\nu} \kappa K_{\mu\nu}^* + \text{h.c.},\end{aligned}\tag{1}$$

where  $A_\mu$ ,  $K_\mu^*$ ,  $K$ , and  $\kappa$  denote the photon, the  $K^*(892, 1^-)$ ,  $K(495, 0^-)$ , and  $\kappa(682, 0^+)$ , respectively [21]. The field-strength tensor for the massive vector meson is defined as  $K_{\mu\nu}^* = \partial_\mu K_\nu^* - \partial_\nu K_\mu^*$ . The values for the coupling constants  $g_{\gamma K^* K}$  are determined from the experimental data [21], which lead to

$$g_{\gamma K^* K}^{\text{charged}} = 0.254 \text{ GeV}^{-1}, \quad g_{\gamma K^* K}^{\text{neutral}} = -0.388 \text{ GeV}^{-1},\tag{2}$$

whereas we use the vector-meson dominance model to determine the values of  $g_{\gamma K^* \kappa}$  [29]:

$$g_{\gamma K^* \kappa}^{\text{charged}} = -0.119 e \text{ GeV}^{-1}, \quad g_{\gamma K^* \kappa}^{\text{neutral}} = -2g_{\gamma K^* \kappa}^{\text{charged}}.\tag{3}$$

Here  $e$  denotes the unit electric charge  $e = \sqrt{4\pi\alpha_E}$  with  $\alpha_E = 1/137.04$ .

The Lagrangians for the photon-baryon-baryon Yukawa interactions are written by

$$\begin{aligned}\mathcal{L}_{\gamma NN} &= -\bar{N} \left[ e_N \not{A} - \frac{e\kappa_N}{2M_N} \sigma_{\mu\nu} \partial^\nu A^\mu \right] N, \\ \mathcal{L}_{\gamma N\Delta} &= e\bar{\Delta}_\mu \left[ \frac{ig_1}{2M_N} \gamma_\nu \gamma_5 + \frac{g_2}{(2M_N)^2} \gamma_5 \partial_\nu \right] N F^{\mu\nu} + \text{h.c.}, \\ \mathcal{L}_{\gamma\Sigma\Sigma} &= -\bar{\Sigma} \left[ e_\Sigma \not{A} - \frac{e\kappa_\Sigma}{2M_N} \sigma_{\mu\nu} \partial^\nu A^\mu \right] \Sigma,\end{aligned}\tag{4}$$

where  $N$ ,  $\Sigma$ , and  $\Delta$  stand for the nucleon,  $\Sigma(1193, 1/2^+)$ , and  $\Delta(1232, 3/2^+)$ , respectively, and  $M_N$  denotes the mass of nucleon. Here  $\kappa_B$  represents the anomalous magnetic moment of baryon  $B$  and its PDG values are given as [21]:

$$\kappa_n = -1.91, \quad \kappa_p = +1.79, \quad \kappa_{\Sigma^-} = -0.16, \quad \kappa_{\Sigma^0} = +0.65, \quad \kappa_{\Sigma^+} = +1.46.\tag{5}$$

The  $\Delta$  field with spin-3/2 is described by the Rarita-Schwinger formalism [30, 31]. We choose the electric and magnetic couplings as  $g_1 = 4.13$  and  $g_2 = 4.74$  using the experimental data for the helicity amplitudes [21, 22].

We define the effective Lagrangians for the meson-baryon-baryon Yukawa interactions as follows:

$$\begin{aligned}
\mathcal{L}_{K^*N\Sigma} &= -g_{K^*N\Sigma} \bar{\Sigma} \left[ \not{K}^* - \frac{\kappa_{K^*N\Sigma}}{2M_N} \sigma_{\mu\nu} \partial^\nu K^{*\mu} \right] N + \text{h.c.}, \\
\mathcal{L}_{KN\Sigma} &= -ig_{KN\Sigma} \bar{\Sigma} \gamma_5 NK + \text{h.c.}, \\
\mathcal{L}_{\kappa N\Sigma} &= -g_{\kappa N\Sigma} \bar{\Sigma} \kappa N + \text{h.c.}, \\
\mathcal{L}_{K^*\Delta\Sigma} &= -\frac{if_{K^*\Delta\Sigma}}{2M_{K^*}} \bar{\Delta}^\mu \gamma^\nu \gamma_5 \Sigma K_{\mu\nu}^* + \text{h.c.},
\end{aligned} \tag{6}$$

where  $\Sigma = \boldsymbol{\tau} \cdot \mathbf{\Sigma}$  in which  $\boldsymbol{\tau}$  indicates the Pauli matrices. The isospin structures of the  $\Delta$  vertices in Eq. (4) and Eq. (6) are given as follows, respectively:

$$\bar{\Delta} I_{4 \times 2}^0 N, \quad \bar{\Delta} \mathbf{I} \cdot \mathbf{\Sigma} K^*, \tag{7}$$

where  $\mathbf{I}$  stand for the isospin transition ( $3/2 \rightarrow 1/2$ ) matrices

$$I^- = \frac{1}{\sqrt{6}} \begin{pmatrix} 0 & 0 \\ 0 & 0 \\ \sqrt{2} & 0 \\ 0 & \sqrt{6} \end{pmatrix}, \quad I^0 = \frac{1}{\sqrt{6}} \begin{pmatrix} 0 & 0 \\ 2 & 0 \\ 0 & 2 \\ 0 & 0 \end{pmatrix}, \quad I^+ = \frac{1}{\sqrt{6}} \begin{pmatrix} \sqrt{6} & 0 \\ 0 & \sqrt{2} \\ 0 & 0 \\ 0 & 0 \end{pmatrix}. \tag{8}$$

The strong coupling constants for the meson and octet baryons can be estimated by the Nijmegen soft-core model (NSC97a) [23], and the corresponding values are presented by

$$g_{K^*N\Sigma} = -2.46, \quad \kappa_{K^*N\Sigma} = -0.47, \quad g_{KN\Sigma} = 4.23, \quad g_{\kappa N\Sigma} = -5.32, \tag{9}$$

whereas we estimate the value of  $f_{K^*\Delta\Sigma}$  using the quark-model prediction and SU(3) flavor symmetry relation:

$$f_{K^*\Delta\Sigma} = -\frac{2M_{K^*}}{M_\rho} f_{\rho N\Delta} = -12.8, \tag{10}$$

with  $f_{\rho N\Delta} = 5.5$  [32].

Now, we are in a position to consider the resonance contributions. First, we write the EM and strong effective Lagrangians with the hyperon resonance  $\Sigma^*$ :

$$\begin{aligned}
\mathcal{L}_{\gamma\Sigma\Sigma^*} &= e \bar{\Sigma}^* \left[ \frac{ig_{\gamma\Sigma\Sigma^*}^V}{2M_N} \gamma_\nu \gamma_5 + \frac{g_{\gamma\Sigma\Sigma^*}^T}{(2M_N)^2} \gamma_5 \partial_\nu \right] \Sigma F^{\mu\nu} + \text{h.c.}, \\
\mathcal{L}_{K^*N\Sigma^*} &= -\frac{if_{K^*N\Sigma^*}^{(1)}}{2M_{K^*}} \bar{K}_{\mu\nu}^* \bar{\Sigma}^{*\mu} \gamma^\nu \gamma_5 N - \frac{f_{K^*N\Sigma^*}^{(2)}}{(2M_{K^*})^2} \bar{K}_{\mu\nu}^* \bar{\Sigma}^{*\mu} \gamma_5 \partial^\nu N + \frac{f_{K^*N\Sigma^*}^{(3)}}{(2M_{K^*})^2} \partial^\nu \bar{K}_{\mu\nu}^* \bar{\Sigma}^{*\mu} \gamma_5 N + \text{h.c.}
\end{aligned} \tag{11}$$

In order to determine  $g_{\gamma\Sigma\Sigma^*}^{V,T}$ , we need to know the experimental data for the  $\Sigma^* \rightarrow \Sigma\gamma$  radiative decay. However, only the upper limits of the hyperon decay rates are known [33]. Moreover,  $\Sigma^{*-} \rightarrow \Sigma^- \gamma$  is known to be  $U$ -spin forbidden, which means its decay rate vanishes in the exact SU(3) symmetry. On the other hand, these decay rates were predicted within several different theoretical frameworks [34–39]. Since Ref. [38] computed the hyperon radiative decay rates as well as  $E2/M1$  ratio, we use the results of Ref. [38], so that we are able to extract  $g_{\gamma\Sigma\Sigma^*}^{V,T}$  as follows:

$$\begin{aligned}
g_{\gamma\Sigma\Sigma^*}^{V+} &= 2.66, \quad g_{\gamma\Sigma\Sigma^*}^{T+} = 0.74, \\
g_{\gamma\Sigma\Sigma^*}^{V0} &= 1.10, \quad g_{\gamma\Sigma\Sigma^*}^{T0} = 0.55, \\
g_{\gamma\Sigma\Sigma^*}^{V-} &= 0.49, \quad g_{\gamma\Sigma\Sigma^*}^{T-} = -0.39.
\end{aligned} \tag{12}$$

The coupling constant  $f_{K^*N\Sigma^*}^{(1)}$  can be determined to be  $-5.21$  by flavor SU(3) symmetry. Because of a lack of experimental and theoretical information on  $f_{K^*N\Sigma^*}^{(2,3)}$ , we do not consider them for brevity in the present work.

In addition to the hyperon resonances, we now include the  $s$ -channel resonance contributions. Here, we consider the  $F_{15}(2000)$ ,  $D_{13}(2080)$ ,  $G_{17}(2190)$ , and  $D_{15}(2200)$  for the nucleon and  $F_{35}(2000)$ ,  $G_{37}(2200)$ , and  $F_{37}(2390)$  for the delta resonances, which are located near the threshold of  $K^*\Sigma$  photoproduction. The relevant EM Lagrangians for those baryon resonances can be written as

$$\mathcal{L}_{\gamma NR_{1/2^\pm}} = \frac{eh_{1R_1}}{2M_N} \bar{N} \Gamma(\mp) \sigma_{\mu\nu} \partial^\nu A^\mu R + \text{h.c.},$$

Resonance	$G_{s,l}$	$g_1$	$\Gamma_R$	$A_1$	$A_3$	$h_1$	$h_2$
$N^*$	$F_{15}(2000)$	-0.2	-0.505	300	-0.018	+0.001	+1.29
	$D_{13}(2080)$	-0.5	-0.238	300	-0.020	+0.017	+0.608
	$G_{17}(2190)$	-0.3	+5.63	300	-0.034	+0.028	+7.70
	$D_{15}(2200)$	+0.2	+1.11	300	-0.002	-0.006	+0.123
$\Delta^*$	$F_{35}(2000)$	+0.1	+0.252	300	-0.010	-0.028	-0.675
	$G_{37}(2200)$	+0.5	$\pm 8.32$	300	+0.014	-0.004	-2.31
	$F_{37}(2390)$	+0.6	$\pm 5.02$	300	+0.024	+0.030	-1.89
$Y^* \quad \Sigma^*(1385, 3/2^+)$	-						

TABLE I. Parameters for the resonances in Eqs. (13) and (15). The decay amplitudes  $G(s, l)$  are computed from Ref. [25]. The full decay widths  $\Gamma_R$  [MeV] and helicity amplitudes  $A_{1,3}$  [ $\text{GeV}^{-\frac{1}{2}}$ ] are taken from the experimental data [21] and theoretical estimations [24]. The (+, -) signs of  $g_1$  for  $G_{37}$  and  $F_{37}$  correspond to their decays to  $(K^{*0}\Sigma^+, K^{*+}\Sigma^0)$ .

$$\begin{aligned}
\mathcal{L}_{\gamma N R_{3/2^\pm}} &= -ie \left[ \frac{h_1}{2M_N} \bar{N} \Gamma_\nu^{(\pm)} - \frac{ih_2}{(2M_N)^2} \partial_\nu \bar{N} \Gamma^{(\pm)} \right] F^{\mu\nu} R_\mu + \text{h.c.}, \\
\mathcal{L}_{\gamma N R_{5/2^\pm}} &= e \left[ \frac{h_1}{(2M_N)^2} \bar{N} \Gamma_\nu^{(\mp)} - \frac{ih_2}{(2M_N)^3} \partial_\nu \bar{N} \Gamma^{(\mp)} \right] \partial^\alpha F^{\mu\nu} R_{\mu\alpha} + \text{h.c.}, \\
\mathcal{L}_{\gamma N R_{7/2^\pm}} &= ie \left[ \frac{h_1}{(2M_N)^3} \bar{N} \Gamma_\nu^{(\pm)} - \frac{ih_2}{(2M_N)^4} \partial_\nu \bar{N} \Gamma^{(\pm)} \right] \partial^\alpha \partial^\beta F^{\mu\nu} R_{\mu\alpha\beta} + \text{h.c.},
\end{aligned} \tag{13}$$

where  $R$  stands for the field corresponding to a nucleon resonance  $R = (N^*, \Delta^*)$  with spin and parity given.  $\Gamma^{(\pm)}$  and  $\Gamma_\nu^{(\pm)}$  in Eq.(13) are defined as

$$\Gamma^{(\pm)} = \begin{pmatrix} \gamma_5 \\ \mathbf{1} \end{pmatrix}, \quad \Gamma_\mu^{(\pm)} = \begin{pmatrix} \gamma_\mu \gamma_5 \\ \gamma_\mu \end{pmatrix}. \tag{14}$$

The coupling constants are determined by using the experimental data for the helicity amplitudes [21, 22] and the quark-model predictions of Ref. [22, 24]. Those for the strong interactions are given as

$$\begin{aligned}
\mathcal{L}_{K^* \Sigma R_{1/2^\pm}} &= -\frac{1}{2M_N} \bar{\Sigma} \left[ g_1 \left( \pm \frac{\Gamma_\mu^{(\mp)} \partial^2}{M_R \mp M_N} - i \Gamma^{(\mp)} \partial_\mu \right) - g_2 \Gamma^{(\mp)} \sigma_{\mu\nu} \partial^\nu \right] K^{*\mu} R + \text{h.c.}, \\
\mathcal{L}_{K^* \Sigma R_{3/2^\pm}} &= -i \left[ \frac{g_1}{2M_N} \bar{\Sigma} \Gamma_\nu^{(\pm)} - \frac{ig_2}{(2M_N)^2} \partial_\nu \bar{\Sigma} \Gamma^{(\pm)} + \frac{ig_3}{(2M_N)^2} \bar{\Sigma} \Gamma^{(\pm)} \partial_\nu \right] K^{*\mu\nu} R_\mu + \text{h.c.}, \\
\mathcal{L}_{K^* \Sigma R_{5/2^\pm}} &= \left[ \frac{g_1}{(2M_N)^2} \bar{\Sigma} \Gamma_\nu^{(\mp)} - \frac{ig_2}{(2M_N)^3} \partial_\nu \bar{\Sigma} \Gamma^{(\mp)} + \frac{ig_3}{(2M_N)^3} \bar{\Sigma} \Gamma^{(\mp)} \partial_\nu \right] \partial^\alpha K^{*\mu\nu} R_{\mu\alpha} + \text{h.c.}, \\
\mathcal{L}_{K^* \Sigma R_{7/2^\pm}} &= i \left[ \frac{g_1}{(2M_N)^3} \bar{\Sigma} \Gamma_\nu^{(\pm)} - \frac{ig_2}{(2M_N)^4} \partial_\nu \bar{\Sigma} \Gamma^{(\pm)} + \frac{ig_3}{(2M_N)^4} \bar{\Sigma} \Gamma^{(\pm)} \partial_\nu \right] \partial^\alpha \partial^\beta K^{*\mu\nu} R_{\mu\alpha\beta} + \text{h.c.},
\end{aligned} \tag{15}$$

where  $M_R$  is the corresponding resonance mass. The strong coupling constants in Eq. (15) can be determined from the theoretical estimations for the partial-wave decay amplitudes [25]:

$$\Gamma_{R \rightarrow K^* \Sigma} = \sum_{s,l} |G(s, l)|^2, \tag{16}$$

where  $\Gamma_{R \rightarrow K^* \Sigma}$  is the decay width of  $R \rightarrow K^* \Sigma$ . The values for the partial-wave coupling strengths  $G(s, l)$  can be found in Ref. [25]. Since the purpose of the present work is to investigate the role of resonances near the threshold, it is enough to take into account the contributions of the lower partial waves. Hence, we consider only the  $g_1$  terms in Eq. (15), employing only the lowest partial-wave contribution for  $G(s, l)$ . Using Eq. (16) and the prediction of Ref. [25], we then can compute the strong coupling constants for the resonances. The signs of these strong coupling constants are determined by fitting the experimental data [12], as will be shown in the next Section. We list all the parameters of the resonances in Table I.

The form factors for each vertex are included in a gauge-invariant manner, so that the invariant amplitudes can be expressed as

$$\mathcal{M} = [\mathcal{M}_{s(N)}^{\text{elec}} + \mathcal{M}_{u(\Sigma)}] F_{\text{com}}^2 + \mathcal{M}_{s(N)}^{\text{mag}} F_N^2 + \mathcal{M}_{t(K)} F_K^2 + \mathcal{M}_{t(\kappa)} F_\kappa^2 + \mathcal{M}_{s(\Delta)} F_\Delta^2$$

$$+\mathcal{M}_{u(\Sigma^*)}F_{\Sigma^*}^2+\mathcal{M}_{s(N^*)}F_{N^*}^2+\mathcal{M}_{s(\Delta^*)}F_{\Delta^*}^2 \quad (17)$$

for the  $K^{*0}\Sigma^+$  and

$$\begin{aligned} \mathcal{M} = & [\mathcal{M}_{t(K^*)}+\mathcal{M}_{s(N)}^{\text{elec}}+\mathcal{M}_c]F_{\text{com}}^2+\mathcal{M}_{s(N)}^{\text{mag}}F_N^2+\mathcal{M}_{t(K)}F_K^2+\mathcal{M}_{t(\kappa)}F_\kappa^2+\mathcal{M}_{s(\Delta)}F_\Delta^2 \\ & +\mathcal{M}_{u(\Lambda)}F_\Lambda^2+\mathcal{M}_{u(\Sigma)}F_\Sigma^2+\mathcal{M}_{u(\Sigma^*)}F_{\Sigma^*}^2+\mathcal{M}_{s(N^*)}F_{N^*}^2+\mathcal{M}_{s(\Delta^*)}F_{\Delta^*}^2 \end{aligned} \quad (18)$$

for the  $K^{*+}\Sigma^0$  channel, respectively. The explicit expressions for each invariant amplitude can be found in Appendix. The common form factor  $F_{\text{com}}$  and those for the off-mass shell meson ( $\Phi$ ) and baryon ( $B$ ) vertices are written generically as

$$F_{\text{com}}=F_N F_{\Sigma(K^*)}-F_N-F_{\Sigma(K^*)}, \quad F_\Phi=\frac{\Lambda_\Phi^2-M_\Phi^2}{\Lambda_\Phi^2-q^2}, \quad F_B=\frac{\Lambda_B^4}{\Lambda_B^4+(q^2-M_B^2)^2}, \quad (19)$$

where  $q$  denotes the off-shell momentum of the relevant hadron in each kinematic channel [26–28]. For the mesonic ( $\Phi = \kappa, K, K^*$ ) and baryonic ( $B = N, \Delta, \Lambda, \Sigma, \Sigma^*, R$ ) vertices, we consider different types of form factors with the cut-off masses  $\Lambda_\Phi$  and  $\Lambda_B$ .

### III. NUMERICAL RESULTS

In this Section, we present and discuss the numerical results. All the calculations are performed in the center-of-mass (CM) frame. The cut-off masses for the phenomenological form factors in Eq. (19) are determined to reproduce the experimental data for the total and differential cross sections for the  $K^{*0}\Sigma^+$  channel from the CBELSA/TAPS [12]. The determined cut-off masses are listed in Table II.

$\Lambda_\Phi$ for $t$ -channel			$\Lambda_B$ for $s$ -channel				$\Lambda_B$ for $u$ -channel		
$\Lambda_{K^*}$	$\Lambda_K$	$\Lambda_\kappa$	$\Lambda_N$	$\Lambda_\Delta$	$\Lambda_{N^*}$	$\Lambda_{\Delta^*}$	$\Lambda_\Lambda$	$\Lambda_\Sigma$	$\Lambda_{\Sigma^*}$
1.10 GeV	1.25 GeV	1.25 GeV	1.50 GeV	1.50 GeV	1.00 GeV	1.00 GeV	0.75 GeV	0.95 GeV	0.95 GeV

TABLE II. Cut-off masses for the form factors in Eq. (19) for each channel.

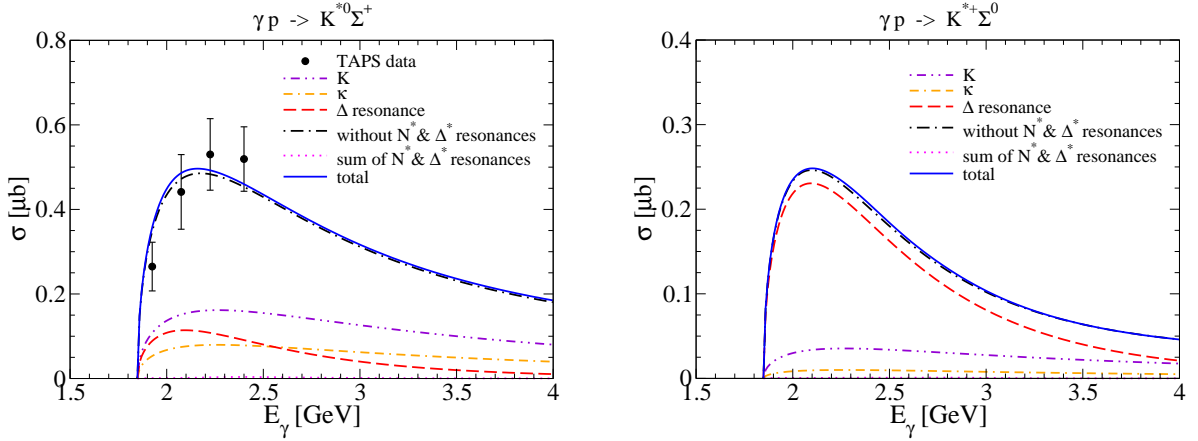


FIG. 2. (Color online) Total cross sections for  $\gamma p \rightarrow K^{*0}\Sigma^+$  as functions of the photon energy  $E_\gamma$  in the left panel. The experimental data of the TAPS collaboration are taken from [12]. The Total cross sections for  $\gamma p \rightarrow K^{*+}\Sigma^0$  are given in the right panel with the same notation.

We draw the numerical results for the total cross sections for the  $K^{*0}\Sigma^+$  channel in the left panel of Fig. 2 in which the  $K$ -,  $\kappa$ -exchange, and  $\Delta$ -pole contributions are depicted in dot-dot-dashed, dash-dash-dotted, and dashed curves, separately. The solid curve designates the total cross section with all contributions included. The experimental data are taken from the TAPS experiment [12]. The results are in a good agreement with the data. It turns out that the  $t$ -channel and the  $\Delta(1232)$ -pole contributions only can describe the experimental data for the  $\gamma p \rightarrow K^{*0}\Sigma^+$  total

cross section as shown in the dot-dashed curve, which indicates that the baryon resonance contributions are almost negligible.

In the right panel of Fig. 2, we show the results for the  $\gamma p \rightarrow K^{*+}\Sigma^0$  process. Note that its production strength is about a half of that of the  $\gamma p \rightarrow K^{*0}\Sigma^+$  one, because of the fact that, even the isospin factor of the  $K^{*+}\Sigma^0\Delta^+$  vertex is larger than that of the  $K^{*0}\Sigma^+\Delta^+$  one:  $I_{K^{*+}\Sigma^0\Delta^+}/I_{K^{*0}\Sigma^+\Delta^+} = \sqrt{2}$ , the  $t$ -channel plays a prominent role in the  $K^{*0}\Sigma^+$  process compared with the  $K^{*+}\Sigma^0$  one as shown in Fig. 2. The other  $N^*$ ,  $\Delta^*$  and hyperon resonances have minute effects on the  $K^{*+}\Sigma^0$  production, being similar to the  $K^{*0}\Sigma^+$  one. Thus, all other resonances except for  $\Delta(1232)$  seems to be unimportant in describing the *unpolarized* cross sections for  $K^*\Sigma$  photoproduction. However, even though these resonances contributions are negligibly tiny, we will see later that they play certain roles in the polarization observables. In particular, they exhibit more sensitive angular dependence than other contributions. These features are obviously distinguished from  $K^*\Lambda$  photoproduction previously examined in Ref. [19]. We also verified that with a different set of the strong coupling constants such as that from the Nijmegen potential (NSC97f) [23] we reached the same conclusion.

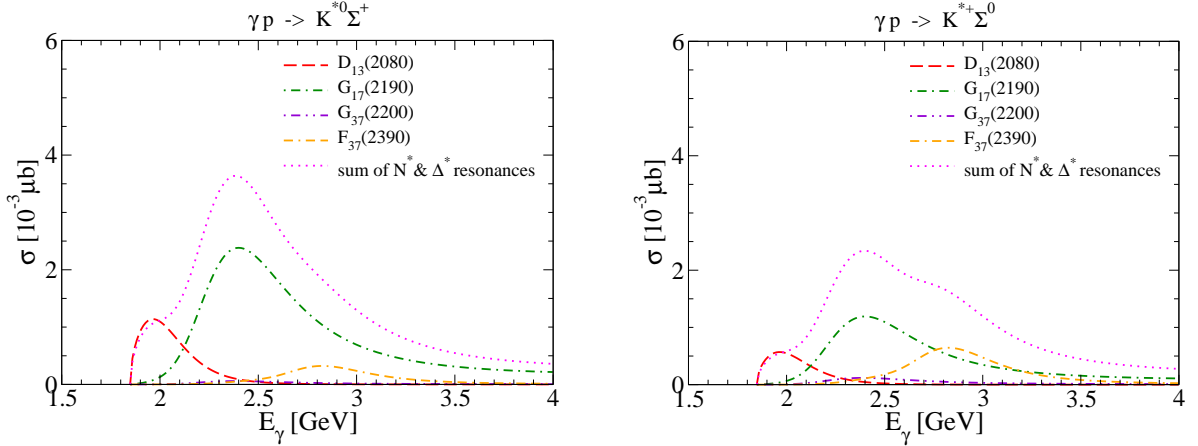


FIG. 3. (Color online)  $N^*$  and  $\Delta^*$  resonance contributions to the total cross sections to  $\gamma p \rightarrow K^{*0}\Sigma^+$  as functions of the photon energy  $E_\gamma$  in the left panel and to  $\gamma p \rightarrow K^{*+}\Sigma^0$  in the right panel with the same notation.

Since the  $N^*$  and  $\Delta^*$  resonances make effects on the polarization observables as we have mentioned already, it is necessary to scrutinize them. In Fig. 3, we draw each contribution of the  $N^*$  ( $D_{13}(2080)$ ,  $G_{17}(2190)$ ) and  $\Delta^*$  ( $G_{37}(2200)$ ,  $F_{37}(2390)$ ) resonances. Though we computed the contributions of the  $F_{15}(2000)$ ,  $D_{15}(2200)$ , and  $F_{35}(2000)$ , we did not show them in Fig. 3, because they are almost negligible. As expected, the magnitude of their contributions is about 100 times smaller than those of the  $t$ -channel and of the  $\Delta$ -pole diagrams. Note that  $D_{13}$  and  $G_{17}$  are pronounced among the resonances. As mentioned already, these features of higher  $N^*$  and  $\Delta^*$  resonances are very different from the case of  $K^*\Lambda$  photoproduction [19], which ensues from the fact that the strong coupling constants of  $\Sigma$  to these resonances are much smaller than those of  $\Lambda$  to them according to the SU(6) quark-model calculations [25]. Comparing explicitly Table II in this work with Table III in Ref. [19], one can easily find the reason, for example,  $g_{K^*\Sigma D_{13}}/g_{K^*\Lambda D_{13}} \sim 1/7$  due to the different isospin factors.

Figure 4 depicts the numerical results for the differential cross sections  $d\sigma/d\cos\theta$  for the  $K^{*0}\Sigma^+$  channel as functions of  $\cos\theta$ . The experimental data are taken from TAPS [12] (solid circle) and CLAS [14] (open square) collaborations measured in the range of the photon energy  $E_\gamma = (1.925 - 2.9125)$  GeV. Note that there is almost no effect from other  $N^*$  and  $\Delta^*$  resonances. Below  $E_\gamma = 2.45$  GeV, the present numerical results reproduce the CLAS and TAPS data qualitatively well, especially in the backward direction ( $\cos\theta < 0$ ). Above  $E_\gamma = 2.6$  GeV, the CLAS data [14] are only available, from which the results show sizable deviation in the forward direction. Theoretically, the forward-scattering enhancements are known to originate mainly from the  $t$ -channel diagrams, i.e.  $\kappa$  and  $K$  exchanges. Although we did not show explicitly in the present work, we checked that the magnetic coupling of the  $\gamma K^{*0}\bar{K}^{*0}$  vertex did not have any meaningful effects on the forward-scattering region. We note that the  $\Delta$ -pole and  $u$ -channel Born contributions are responsible for the enhancement in the backward angle.

We also illustrate the differential cross sections for the  $\gamma p \rightarrow K^{*+}\Sigma^0$  process in Fig. 5 in the same manner as in Fig. 4. As understood from Fig. 2, the overall strengths of the differential cross sections are smaller than those of the  $K^{*0}\Sigma^+$  channel. Since there are the  $K^*$ -exchange, the  $\Lambda$ -exchange, and the contact-term in addition to other diagrams so as to satisfy the WT identity, the angular dependence of the differential cross sections for  $K^{*+}\Sigma^0$  photoproduction turns out to be rather different from those for  $K^{*+}\Sigma^0$ . In general, the results fall off slowly as  $\cos\theta$  decreases due

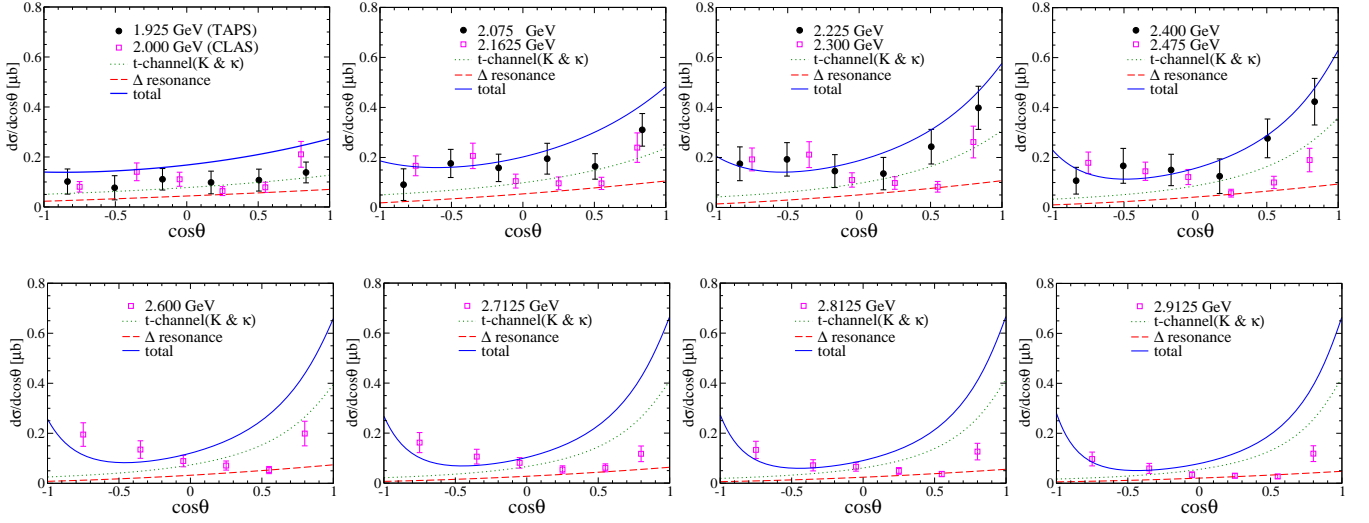


FIG. 4. (Color online) Differential cross sections for  $\gamma p \rightarrow K^{*0}\Sigma^+$  as functions of  $\cos\theta$  for different photon energies ( $E_\gamma$ ) in the range (1.925 – 2.9125) GeV. The dotted curve shows the  $t$ -channel effects ( $K$  and  $\kappa$  exchanges), whereas the dashed curve draws the  $\Delta$ -pole contribution. The solid curve represents the total result. The experimental data of the TAPS and CLAS collaborations are taken from Ref. [12] and Ref. [14], respectively.

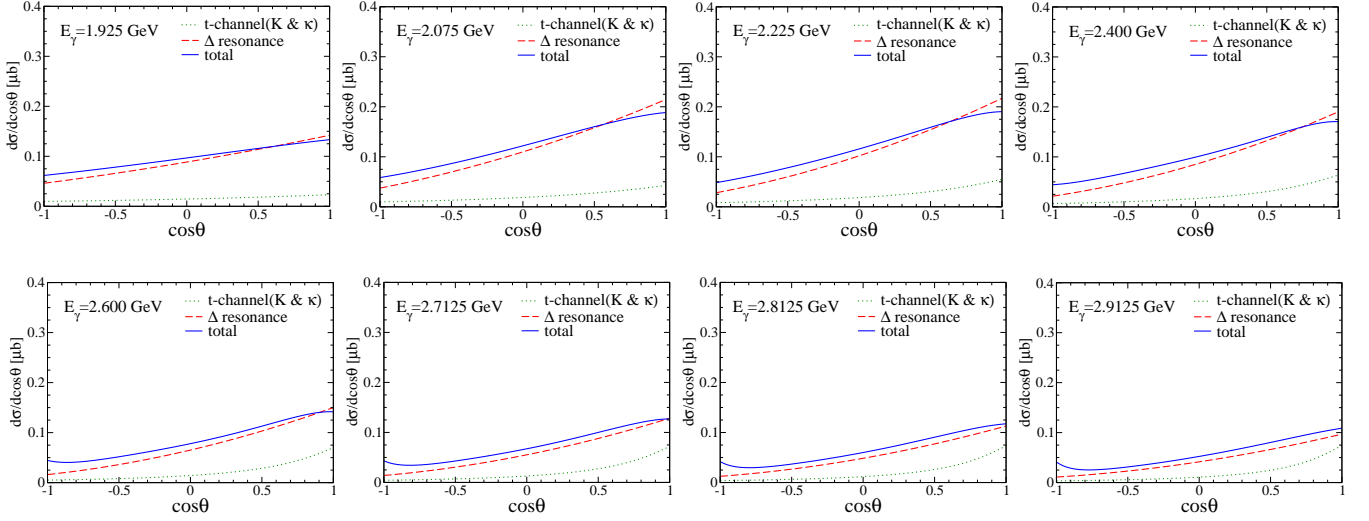


FIG. 5. (Color online) Differential cross sections for  $\gamma p \rightarrow K^{*+}\Sigma^0$  as functions of  $\cos\theta$  for different photon energies ( $E_\gamma$ ) in the range (1.925 – 2.9125) GeV. The dotted curve shows the  $t$ -channel effects ( $K$  and  $\kappa$  exchanges), whereas the dashed curve draws the  $\Delta$ -pole contribution. The solid curve represents the total result.

to the dominant  $\Delta$ -pole, additional  $K^*$ -exchange, and contact-term diagrams. When  $E_\gamma$  is larger than 2.4 GeV, the  $\gamma p \rightarrow K^{*+}\Sigma^0$  differential cross section slightly increases as  $\cos\theta$  approaches  $-1$ .

We are now in a position to discuss the single polarization observables. The photon-beam  $\Sigma_\gamma$ , recoil  $P_y$ , target  $T_y$  asymmetries are defined as follows [40]:

$$\Sigma_\gamma \equiv \frac{d\sigma(\epsilon_\perp) - d\sigma(\epsilon_\parallel)}{d\sigma_{\text{unpol.}}}, \quad P_y \equiv \frac{d\sigma(s_y^\Sigma = \frac{1}{2}) - d\sigma(s_y^\Sigma = -\frac{1}{2})}{d\sigma_{\text{unpol.}}}, \quad T_y \equiv \frac{d\sigma(s_y^N = \frac{1}{2}) - d\sigma(s_y^N = -\frac{1}{2})}{d\sigma_{\text{unpol.}}}, \quad (20)$$

where  $d\sigma_{\text{unpol.}}$  stands for the unpolarized differential cross section. These polarization observables quantities satisfy the following conditions in the collinear limit:

$$\Sigma_\gamma = P_y = T_y = 0 \text{ at } \cos\theta = \pm 1. \quad (21)$$

Throughout the present work, we define the reaction plane by the  $x$ - $z$  axes. Thus, the  $y$  axis is perpendicular to the

reaction plane. The photon polarization vectors  $\epsilon_\perp$  and  $\epsilon_\parallel$  are defined in Appendix, while  $s_y^B$  indicates the spin of a baryon  $B$  along the  $y$  direction.

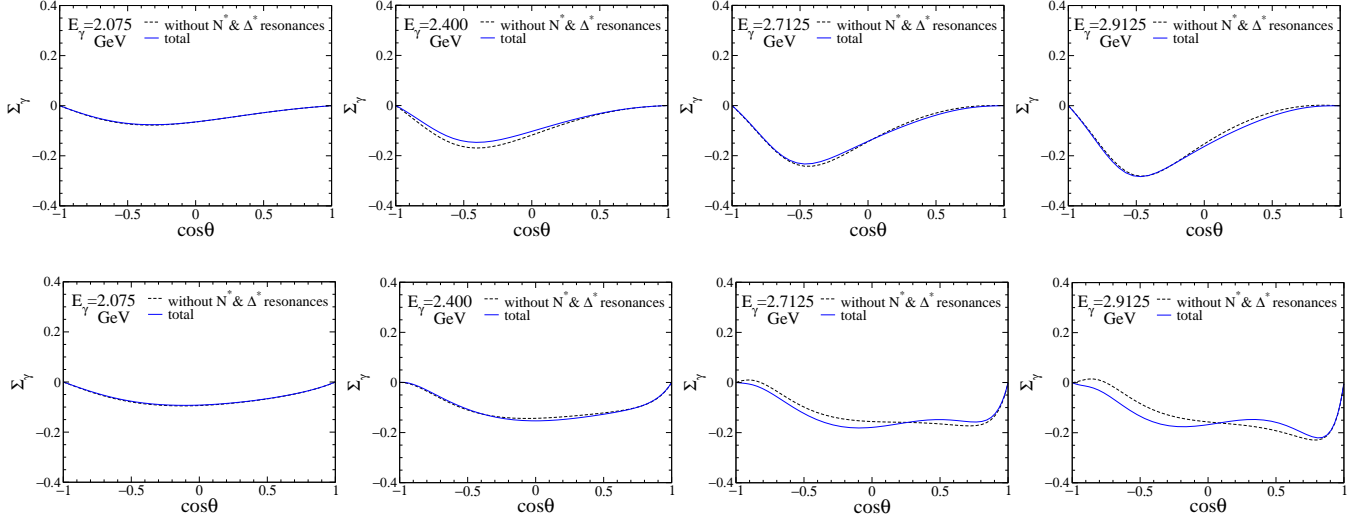


FIG. 6. (Color online) In the upper panel, photon-beam asymmetry  $\Sigma_\gamma$  for  $\gamma p \rightarrow K^{*0}\Sigma^+$  as functions of  $\cos\theta$  in the range of  $E_\gamma = (2.075 - 2.9125)$  GeV. The solid and dashed curves represent the results with and without the resonance contributions, respectively. In the lower panel, photon-beam asymmetry  $\Sigma_\gamma$  for  $\gamma p \rightarrow K^{*+}\Sigma^0$  with the same notation.

In Fig. 6, we depict the numerical results of  $\Sigma_\gamma$  for  $K^{*0}\Sigma^+$  in the upper panel and for  $K^{*+}\Sigma^0$  in the lower panel as functions of  $\cos\theta$  in the range of  $E_\gamma = (2.075 - 2.9125)$  GeV. In Fig. 6 it is found that the  $N^*$  and  $\Delta^*$  resonances does not much affect the  $\Sigma_\gamma$  for both  $K^*\Sigma$  photoproductions, which was already seen for the differential cross sections as shown in Fig. 5. While  $\kappa$  and  $K$  exchanges govern the  $K^{*0}\Sigma^+$  production mechanism because of their large magnetic couplings, the  $\Delta$ -pole contribution in the  $s$ -channel pulls down the  $\Sigma_\gamma$  to the negative direction. The effect of the  $\Delta$ -pole contribution becomes larger as  $E_\gamma$  increases. The dependence of  $\Sigma_\gamma$  on  $\cos\theta$  is more complicated in the case of the  $K^{*+}\Sigma^0$  production, in particular, for higher  $E_\gamma$ , as illustrated in the lower panel of Fig. 6. As mentioned previously, the  $K^*$ -exchange and contact-term also contribute to the  $\gamma p \rightarrow K^{*+}\Sigma^0$  process. Moreover, in the case of  $\Sigma_\gamma$ , the electric couplings of these diagrams enhance  $\Sigma_\gamma$  to its positive region, in addition to the dominant  $\Delta$ -pole one.

In the upper panel of Fig. 7, we draw the photon-beam asymmetries for  $K^{*0}\Sigma^+$  photoproduction with and without  $N^*$  and  $\Delta^*$  resonances in order as functions of  $E_\gamma$ , the scattering angle being varied between  $\theta = 0^\circ$  and  $\theta = 180^\circ$ . In the lower panel,  $\Sigma_\gamma$  for the  $K^{*+}\Sigma^0$  channel are depicted in the same notation as for  $\gamma p \rightarrow K^{*0}\Sigma^+$ . Though the effects of the  $N^*$  and  $\Delta^*$  resonances seem to be small, one can see slight change of  $\Sigma_\gamma$  as  $E_\gamma$  increases. In particular, the effects are visible at  $\theta = 120^\circ$ . In the case of  $K^{*+}\Sigma^0$  production, the influence of the higher resonances is more clearly revealed in the intermediate angles ( $\theta = 60 - 120^\circ$ ).

In the upper panel of Fig. 8, the recoil asymmetries  $P_y$  for  $\gamma p \rightarrow K^{*0}\Sigma^+$  is presented as functions of  $\cos\theta$  in the range of the photon energy  $E_\gamma = 2.075 - 2.9125$  GeV. The solid and dashed curves illustrate the results of  $P_y$  with and without the  $N^*$  and  $\Delta^*$  resonances. We observe that the higher resonances have some effects on  $P_y$ , in contradiction with the case of  $\Sigma_\gamma$ . Figure 8 shows that  $P_y$  stay almost zero in the whole range of  $E_\gamma$ . By introducing the  $N^*$  and  $\Delta^*$  resonances, we find that in the  $K^{*0}\Sigma^+$  channel  $P_y$  exhibits strong dependence on  $\theta$ . Since the  $N^*$  resonances we have considered have rather large spins, their effects on recoil and target asymmetries that are defined as the subtraction between the polarized differential cross sections with opposite spin directions of the baryons concerned are expected to be natural. Moreover, the contributions of the  $N^*$  resonances are amplified as  $E_\gamma$  increases, as shown in the upper panel of Fig. 8. In the lower panel of Fig. 8,  $P_y$  for  $K^{*+}\Sigma^0$  photoproduction are depicted. In this case, the effects of the higher resonances are mild in the lower  $E_\gamma$  region. However, as  $E_\gamma$  increase,  $P_y$  starts to show again strong dependence on the scattering angle.

Figure 9 draws  $P_y$  as functions of  $E_\gamma$  for the  $K^{*0}\Sigma^+$  channel in the upper panel with and without the  $N^*$  and  $\Delta^*$  resonances in order and for the  $K^{*+}\Sigma^0$  channel in the lower one in the same way. The scattering angle is changed from  $0^\circ$  to  $180^\circ$ . When the effects of the higher resonances are turned off,  $P_y$  is in general almost independent of  $E_\gamma$ . Only at  $\theta = 60^\circ$ ,  $P_y$  increases as  $E_\gamma$  does. The increase of  $P_y$  is more visible in the  $K^{*+}\Sigma^0$  case. However, including the higher resonances, we find that  $P_y$  at  $\theta = 60^\circ$  starts to rise until  $E_\gamma \approx 2.2$  GeV and then falls off slowly, as  $E_\gamma$  increases. On the other hand,  $P_y$  at  $\theta = 60^\circ$  for the  $K^{*+}\Sigma^0$  channel begins to increase around 2.1 GeV and then

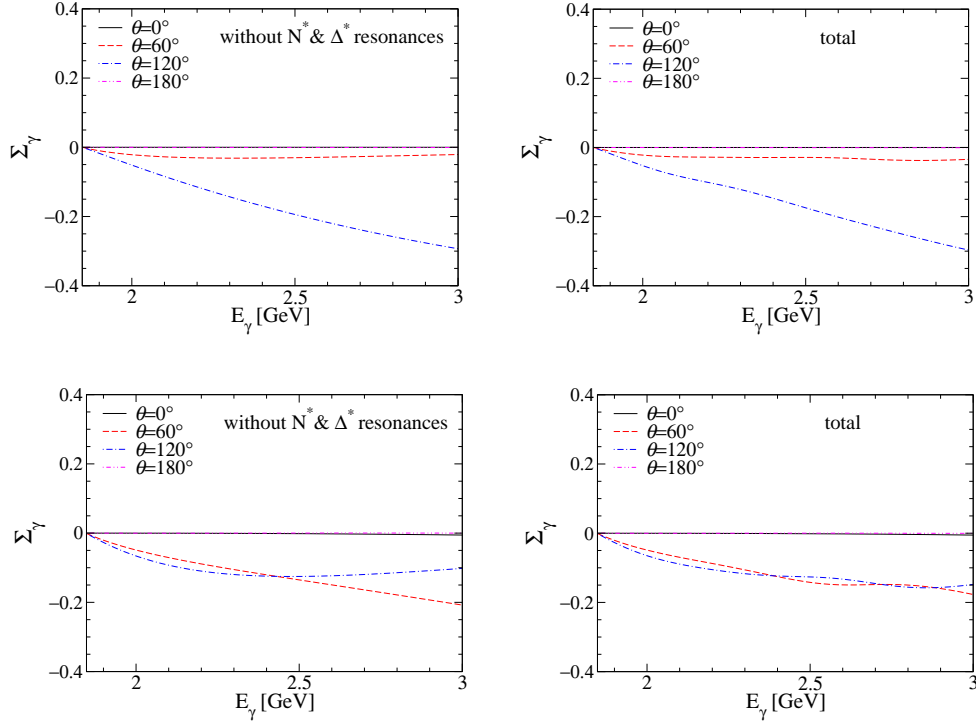


FIG. 7. (Color online) In the upper panel, photon-beam asymmetries  $\Sigma_\gamma$  for  $\gamma p \rightarrow K^{*0}\Sigma^+$  with and without  $N^*$  and  $\Delta^*$  resonances are drawn in order as functions of the photon energy  $E_\gamma$ , the scattering angle being changed from  $0^\circ$  to  $180^\circ$ . In the lower panel, those for  $\gamma p \rightarrow K^{*+}\Sigma^0$  are shown with and without the resonance contributions, respectively.

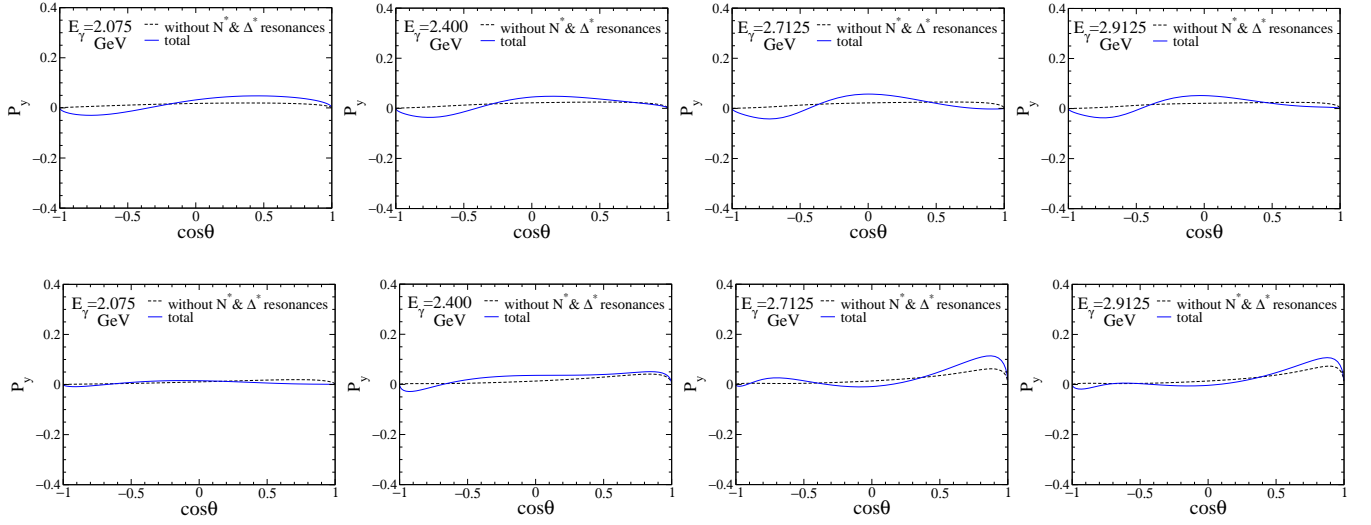


FIG. 8. (Color online) Recoil asymmetries  $P_y$  for  $K^*\Sigma$  photoproduction as functions of  $\cos\theta$  in the range of the photon energy  $E_\gamma = 2.075 - 2.9125$  GeV. In the upper and lower panels,  $P_y$  are drawn for the  $K^{*0}\Sigma^+$  and  $K^{*+}\Sigma^0$  productions, respectively. The solid and dashed curves stand for the results with and without the  $N^*$  and  $\Delta^*$  resonances, respectively.

saturates around 2.5 GeV.

Finally, we provide the numerical results for the target asymmetries  $T_y$  in Fig. 10 as functions of  $\cos\theta$  in the same manner as in Fig. 8. As shown in Fig. 10, the effects of the higher resonances on  $T_y$  tend to be very similar to those on  $P_y$ . Interestingly, however, we find that the phases of the  $T_y$  curves for the  $K^{*0}\Sigma^+$  and  $K^{*+}\Sigma^0$  are reversed each other.

The dependence of  $T_y$  on  $E_\gamma$  is shown in Fig. 11 in the same way as Fig. 9. Again, it turns out that the higher resonance contributions become obvious around  $E_\gamma = (2.0 \sim 2.5)$  GeV, due to the similar reason for  $P_y$ .

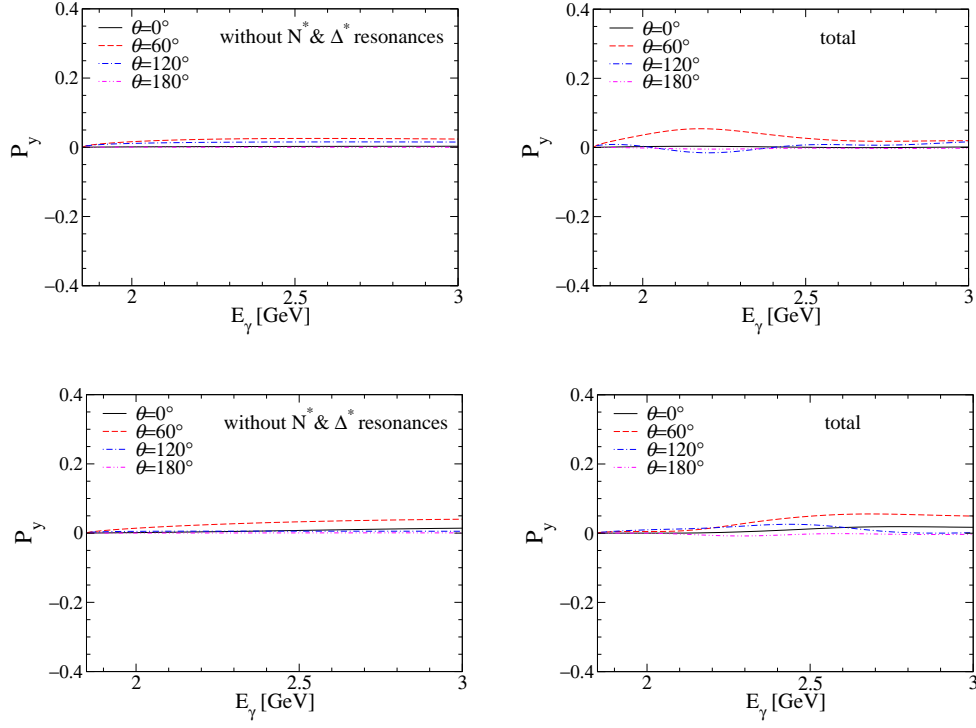


FIG. 9. (Color online) In the upper panel, recoil asymmetries  $P_y$  for  $\gamma p \rightarrow K^{*0}\Sigma^+$  with and without  $N^*$  and  $\Delta^*$  resonances are drawn in order as functions of the photon energy  $E_\gamma$ , the scattering angle being changed from  $0^\circ$  to  $180^\circ$ . In the lower panel, those for  $\gamma p \rightarrow K^{*+}\Sigma^0$  are shown with and without the resonance contributions, respectively.

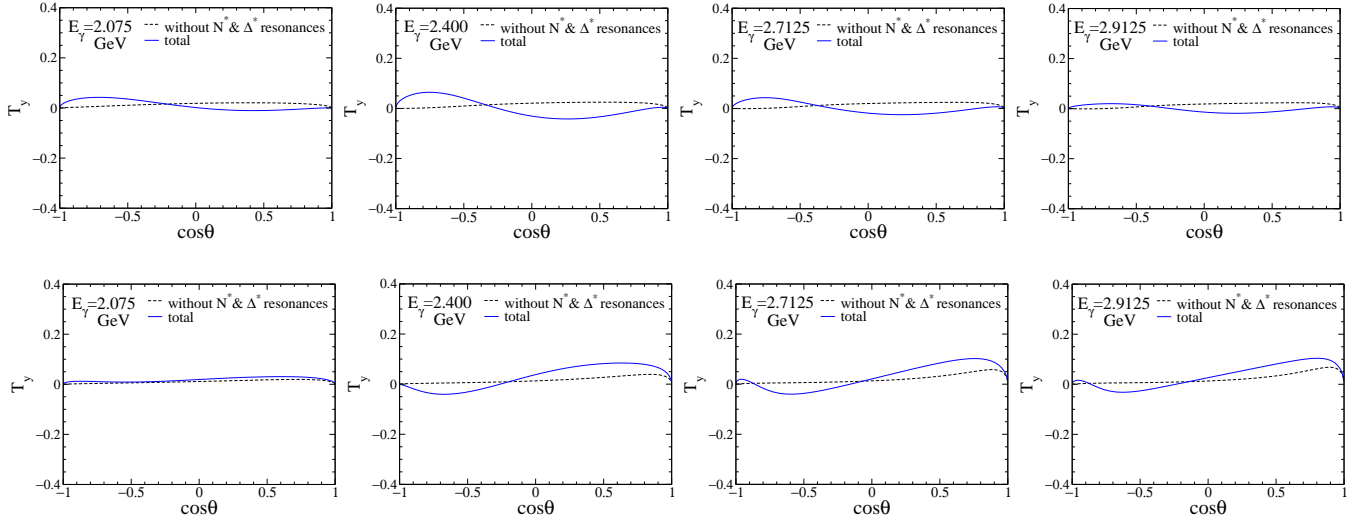


FIG. 10. (Color online) Target asymmetries  $T_y$  for  $K^*\Sigma$  photoproduction as functions of  $\cos\theta$  in the range of the photon energy  $E_\gamma = 2.075 - 2.9125$  GeV. In the upper and lower panels,  $T_y$  are drawn for the  $K^{*0}\Sigma^+$  and  $K^{*+}\Sigma^0$  productions, respectively. The solid and dashed curves stand for the results with and without the  $N^*$  and  $\Delta^*$  resonances, respectively.

#### IV. SUMMARY AND CONCLUSION

We have investigated the  $K^*\Sigma(1193)$  photoproduction, employing the effective Lagrangian approach at the tree-level Born approximation. In addition to the Born diagrams, which satisfy the WT identity with the phenomenological form factors, we took into account the baryon resonance contributions in the  $s$ - and  $u$ -channels. All the model parameters were determined by using experimental and theoretical information, the available experimental data for the present reaction process being reproduced. We summarize important observations in the present work as follows:

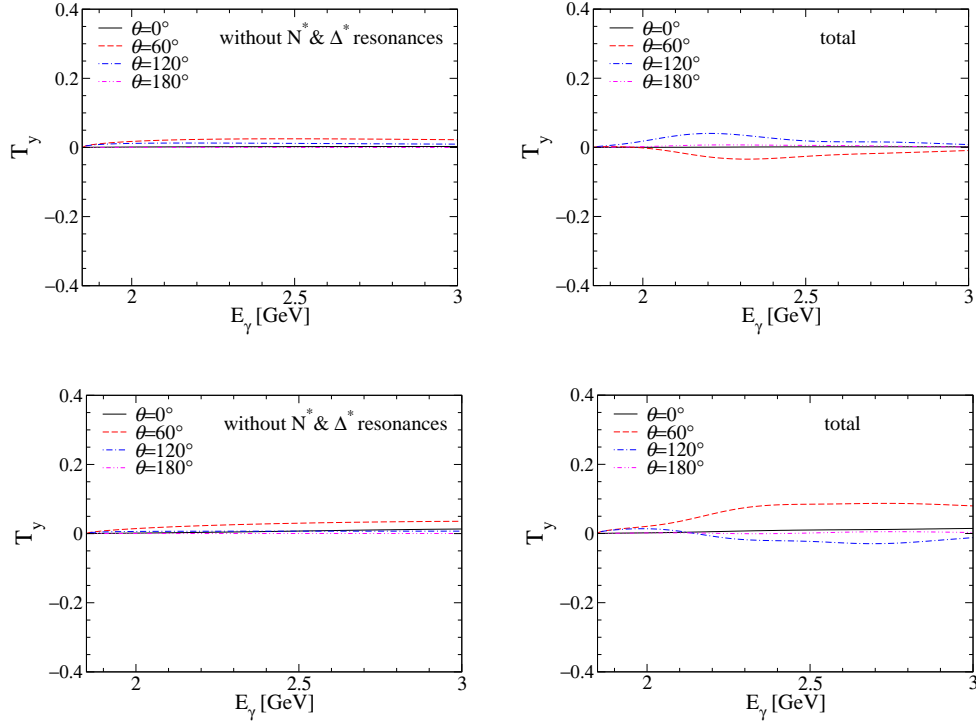


FIG. 11. (Color online) In the upper panel, target asymmetries  $T_y$  for  $\gamma p \rightarrow K^{*0}\Sigma^+$  with and without  $N^*$  and  $\Delta^*$  resonances are drawn in order as functions of the photon energy  $E_\gamma$ , the scattering angle being changed from  $0^\circ$  to  $180^\circ$ . In the lower panel, those for  $\gamma p \rightarrow K^{*+}\Sigma^0$  are shown with and without the resonance contributions, respectively.

- The unpolarized production strengths for  $K^{*0}\Sigma^+$  and  $K^{*+}\Sigma^0$  photoproductions are negligibly affected by the resonance contributions. In other words, the total production rate is dominated by the Born diagrams such as the  $\Delta$ -pole and  $t$ -channel exchanges, as far as we rely on presently available experimental and theoretical information for the resonances taken into account. This tendency is obviously different from those for  $K\Lambda(1116)$  [4] and  $K^*\Lambda(1116)$  [19] photoproductions. The total cross section of the  $\gamma p \rightarrow K^{*+}\Sigma^0$  process turns out to be about twice smaller than that of  $\gamma p \rightarrow K^{*0}\Sigma^+$ , because of the isospin factors and the coupling constants.
- The angular dependences of the  $K^{*0}\Sigma^+$  channel are qualitatively well reproduced for the TAPS [12] and CLAS [14] experiment data. However, considerable deviations in the forward scattering region were observed, in comparison to the CLAS data beyond  $E_\gamma = 2.5$  GeV. On the contrary, the  $K^{*+}\Sigma^0$  channel angular distribution is dominated by the  $\Delta$ -pole contribution in the  $s$ -channel, showing rather flat curves. Moreover, complicated interference between the  $t$ -channel exchange and the contact-term contributions results in decreasing curves in the very forward-scattering region, whereas there appears monotonic increasing of the curves for the  $K^{*0}\Sigma^+$  channel.
- The single-polarization observables such as recoil and target asymmetries  $P_y$  and  $T_y$  are mainly described by the  $N^*$  resonances, though their effects are almost invisible in the cross sections. The reason lies in the fact that the generic Born and  $\Delta(1232)$ -exchange contributions play a minor role in the polarized observables. On the contrary, it is difficult to see the resonance contributions in the transversely-polarized photon-beam asymmetry  $\Sigma_\gamma$ , since the electric and magnetic coupling strengths for the  $\gamma NR$ , where  $R \equiv (N^*, \Delta^*, Y^*)$ , are qualitatively similar to each other.

As noted above, the  $K^*\Sigma(1193)$  photoproduction manifests obviously different features for the resonance contributions in comparison to other strangeness productions. The present theoretical results, especially the single-polarization observables will be a useful guide for the future experiments in understanding the role of higher resonances in the context of photoproductions, which can be measured by CLAS, LEPS, and TAPS collaborations. The double polarization observables such as the polarization transport coefficients  $C_{x,y}$  [41, 42], are under progress and appear elsewhere.

## ACKNOWLEDGMENT

The authors are grateful to Y. Oh, K. Hicks and W. Tang for fruitful discussions and comments for the present work. The works of S.H.K. and H.Ch.K. were supported by Basic Science Research Program through the National Research Foundation of Korea funded by the Ministry of Education, Science and Technology (Grant Number: 2012001083). S.H.K. is also supported by the Ministry of Education, Culture, Science and Technology of Japan. A.H. is supported in part by the Grant-in-Aid for Scientific Research on Priority Areas titled ‘‘Elucidation of New Hadrons with a Variety of Flavors’’ (E01:21105006).

## APPENDIX

The scattering amplitude for this production can be written as follows:

$$\mathcal{M} = \varepsilon_\nu^* \bar{u}_\Sigma \mathcal{M}^{\mu\nu} u_N \epsilon_\mu, \quad (22)$$

where the Dirac spinors of the nucleon and  $\Lambda$  are denoted by  $u_N$  and  $u_\Sigma$ , respectively, and  $\epsilon_\mu$  and  $\varepsilon_\mu$  represent the polarization vectors for the incoming photon and outgoing  $K^*$ , respectively, as follows:

$$\epsilon_\mu = \begin{cases} \epsilon_\parallel = (0, 1, 0, 0) \\ \epsilon_\perp = (0, 0, 1, 0) \end{cases}, \quad \varepsilon_\mu = \begin{cases} \varepsilon_1 = (0, \cos \theta, 0, -\sin \theta) \\ \varepsilon_2 = (0, 0, 1, 0) \\ \varepsilon_3 = \frac{1}{M_{K^*}} (\mathbf{k}_{K^*}, E_{K^*} \sin \theta, 0, E_{K^*} \cos \theta) \end{cases}, \quad (23)$$

satisfying  $\epsilon^2 = \varepsilon^2 = -1$ , otherwise zero.

The relevant invariant amplitudes for each kinematic channel without  $(N^*, \Delta^*)$  are given as follows:

$$\begin{aligned} \mathcal{M}_c^{\mu\nu} &= -\frac{ie_{K^*} g_{K^* N \Sigma} g_{K^* N \Sigma}}{2M_N} \sigma^{\mu\nu}, \\ \mathcal{M}_{t(\kappa)}^{\mu\nu} &= \frac{-2g_{\gamma K^* \kappa} g_{\kappa N \Sigma}}{t - (M_\kappa - i\Gamma_\kappa/2)^2} (k_1 \cdot k_2 g^{\mu\nu} - k_1^\nu k_2^\mu), \\ \mathcal{M}_{t(K)}^{\mu\nu} &= \frac{ig_{\gamma K K^*} g_{K N \Sigma}}{t - M_K^2} \epsilon^{\mu\nu\alpha\beta} k_{1\alpha} k_{2\beta} \gamma_5, \\ \mathcal{M}_{t(K^*)}^{\mu\nu} &= \frac{e_{K^*} g_{K^* N \Sigma}}{t - (M_{K^*} - i\Gamma_{K^*}/2)^2} (2k_2^\mu g^{\nu\alpha} - k_2^\alpha g^{\mu\nu} + k_1^\nu g^{\mu\alpha}) \left[ g_{\alpha\beta} - \frac{(k_1 - k_2)_\alpha (k_1 - k_2)_\beta}{M_{K^*}^2} \right] \\ &\quad \times \left[ \gamma^\beta - \frac{i\kappa_{K^* N \Sigma}}{2M_N} \sigma^{\beta\delta} (k_1 - k_2)_\delta \right], \\ \mathcal{M}_{s(N)}^{\mu\nu} &= \frac{g_{K^* N \Sigma}}{s - M_N^2} \left[ \gamma^\nu - \frac{i\kappa_{K^* N \Sigma}}{2M_N} \sigma^{\nu\alpha} k_{2\alpha} \right] (\not{k}_1 + \not{p}_1 + M_N) \left[ e_N \gamma^\mu + \frac{ie\kappa_N}{2M_N} \sigma^{\mu\beta} k_{1\beta} \right], \\ \mathcal{M}_{s(\Delta)}^{\mu\nu} &= \frac{f_{K^* \Delta \Sigma}}{s - M_\Delta^2} \frac{e}{2M_{K^*}} \gamma_\rho \gamma_5 (k_2^\beta g^{\nu\rho} - k_2^\rho g^{\nu\beta}) \Delta_{\beta\alpha} \left[ \frac{g_1}{2M_N} \gamma_\delta - \frac{g_2}{(2M_N)^2} p_{1\delta} \right] \gamma_5 (k_1^\alpha g^{\mu\delta} - k_1^\delta g^{\mu\alpha}), \\ \mathcal{M}_{u(\Sigma)}^{\mu\nu} &= \frac{g_{K^* N \Sigma}}{u - M_\Sigma^2} \left[ e_\Sigma \gamma^\mu + \frac{ie\kappa_\Sigma}{2M_N} \sigma^{\mu\alpha} k_{1\alpha} \right] (\not{p}_2 - \not{k}_1 + M_\Sigma) \left[ \gamma^\nu - \frac{i\kappa_{K^* N \Sigma}}{2M_N} \sigma^{\nu\beta} k_{2\beta} \right]. \end{aligned} \quad (24)$$

Now, we write the corresponding invariant amplitudes for  $(N^*, \Delta^*)$  for each spin and parity:

$$\begin{aligned} \mathcal{M}_{s(R)}^{\mu\nu} \left( \frac{1^\pm}{2} \right) &= \frac{-ie}{s - M_R^2} \frac{h_{1R_1}}{(2M_N)^2} \left[ g_1 \frac{M_{K^*}^2}{M_R \mp M_N} \Gamma^{\nu(\mp)} \mp ig_2 \Gamma^{(\mp)} \sigma^{\nu\beta} k_{2\beta} \right] (\not{k}_1 + \not{p}_1 + M_R) \Gamma^{(\mp)} \sigma^{\mu\alpha} k_{1\alpha}, \\ \mathcal{M}_{s(R)}^{\mu\nu} \left( \frac{3^\pm}{2} \right) &= \frac{e}{s - M_R^2} \left[ \frac{g_1}{2M_N} \Gamma_\rho^{(\pm)} + \frac{g_2}{(2M_N)^2} p_{2\rho} \Gamma^{(\pm)} - \frac{g_3}{(2M_N)^2} k_{2\rho} \Gamma^{(\pm)} \right] (k_2^\beta g^{\nu\rho} - k_2^\rho g^{\nu\beta}) \\ &\quad \times \Delta_{\beta\alpha}(R, k_1 + p_1) \left[ \frac{\mu_{R_3}}{2M_N} \Gamma_\delta^{(\pm)} \mp \frac{\bar{\mu}_{R_3}}{(2M_N)^2} \Gamma^{(\pm)} p_{1\delta} \right] (k_1^\alpha g^{\mu\delta} - k_1^\delta g^{\mu\alpha}), \\ \mathcal{M}_{s(R)}^{\mu\nu} \left( \frac{5^\pm}{2} \right) &= \frac{e}{s - M_R^2} \left[ \frac{g_1}{(2M_N)^2} \Gamma_\rho^{(\mp)} + \frac{g_2}{(2M_N)^3} p_{2\rho} \Gamma^{(\mp)} - \frac{g_3}{(2M_N)^3} k_{2\rho} \Gamma^{(\mp)} \right] k_2^{\beta_2} (k_2^{\beta_1} g^{\nu\rho} - k_2^\rho g^{\nu\beta_1}) \\ &\quad \times \Delta_{\beta_1\beta_2;\alpha_1\alpha_2}(R, k_1 + p_1) \left[ \frac{\mu_{R_5}}{(2M_N)^2} \Gamma_\delta^{(\mp)} \pm \frac{\bar{\mu}_{R_5}}{(2M_N)^3} \Gamma^{(\mp)} p_{1\delta} \right] k_1^{\alpha_2} (k_1^{\alpha_1} g^{\mu\delta} - k_1^\delta g^{\mu\alpha_1}), \\ \mathcal{M}_{s(R)}^{\mu\nu} \left( \frac{7^\pm}{2} \right) &= \frac{e}{s - M_R^2} \left[ \frac{g_1}{(2M_N)^3} \Gamma_\rho^{(\pm)} + \frac{g_2}{(2M_N)^4} p_{2\rho} \Gamma^{(\pm)} - \frac{g_3}{(2M_N)^4} k_{2\rho} \Gamma^{(\pm)} \right] k_2^{\beta_2} k_2^{\beta_3} (k_2^{\beta_1} g^{\nu\rho} - k_2^\rho g^{\nu\beta_1}) \end{aligned}$$

$$\begin{aligned}
& \times \Delta_{\beta_1\beta_2\beta_3;\alpha_1\alpha_2\alpha_3}(R, k_1 + p_1) \left[ \frac{\mu_{R7}}{(2M_N)^3} \Gamma_\delta^{(\pm)} \mp \frac{\bar{\mu}_{R7}}{(2M_N)^4} \Gamma^{(\pm)} p_{1\delta} \right] k_1^{\alpha_2} k_1^{\alpha_3} (k_1^{\alpha_1} g^{\mu\delta} - k_1^\delta g^{\alpha_1\mu}), \\
\mathcal{M}_{u(R)}^{\mu\nu} \left( \frac{3^+}{2} \right) &= \frac{f_{K^*N\Sigma^*}^{(1)}}{u - M_{\Sigma^*}^2} \frac{e}{2M_{K^*}} \left[ \frac{g_1}{2M_N} \gamma_\rho + \frac{g_2}{(2M_N)^2} p_{2\rho} \right] (k_1^\beta g^{\rho\mu} - k_1^\rho g^{\beta\mu}) \gamma_5 \Delta_{\beta\alpha} \gamma_\delta \gamma_5 (k_2^\alpha g^{\nu\delta} - k_2^\delta g^{\alpha\nu}),
\end{aligned} \tag{25}$$

where the definitions for  $\Gamma^{(\pm)}$  are given in Eq. (14) and each of the decay widths of resonances is included by replacing  $M_R$  in the propagator with  $M_R - i\Gamma_R/2$ . The spin-3/2, -5/2 and -7/2 Rarita-Schwinger spin projections in Eqs. (24) and (25) are given by

$$\begin{aligned}
\Delta_{\beta\alpha}(R, p) &= (\not{p} + M_R) \left[ -g_{\beta\alpha} + \frac{1}{3} \gamma_\beta \gamma_\alpha + \frac{1}{3M_R} (\gamma_\beta p_\alpha - \gamma_\alpha p_\beta) + \frac{2}{3M_R^2} p_\beta p_\alpha \right], \\
\Delta_{\beta_1\beta_2;\alpha_1\alpha_2}(R, p) &= (\not{p} + M_R) \\
&\times \left[ \frac{1}{2} (\bar{g}_{\beta_1\alpha_1} \bar{g}_{\beta_2\alpha_2} + \bar{g}_{\beta_1\alpha_2} \bar{g}_{\beta_2\alpha_1}) - \frac{1}{5} \bar{g}_{\beta_1\beta_2} \bar{g}_{\alpha_1\alpha_2} - \frac{1}{10} (\bar{\gamma}_{\beta_1} \bar{\gamma}_{\alpha_1} \bar{g}_{\beta_2\alpha_2} + \bar{\gamma}_{\beta_1} \bar{\gamma}_{\alpha_2} \bar{g}_{\beta_2\alpha_1} + \bar{\gamma}_{\beta_2} \bar{\gamma}_{\alpha_1} \bar{g}_{\beta_1\alpha_2} + \bar{\gamma}_{\beta_2} \bar{\gamma}_{\alpha_2} \bar{g}_{\beta_1\alpha_1}) \right], \\
\Delta_{\beta_1\beta_2\beta_3;\alpha_1\alpha_2\alpha_3}(R, p) &= (\not{p} + M_R) \\
&\times \frac{1}{36} \sum_{P(\alpha), P(\beta)} \left[ -\bar{g}_{\beta_1\alpha_1} \bar{g}_{\beta_2\alpha_2} \bar{g}_{\beta_3\alpha_3} + \frac{3}{7} \bar{g}_{\beta_1\alpha_1} \bar{g}_{\beta_2\beta_3} \bar{g}_{\alpha_2\alpha_3} + \frac{3}{7} \bar{\gamma}_{\beta_1} \bar{\gamma}_{\alpha_1} \bar{g}_{\beta_2\alpha_2} \bar{g}_{\beta_3\alpha_3} - \frac{3}{35} \bar{\gamma}_{\beta_1} \bar{\gamma}_{\alpha_1} \bar{g}_{\beta_2\beta_3} \bar{g}_{\alpha_2\alpha_3} \right].
\end{aligned} \tag{26}$$

Here, we have used the following notations for convenience:

$$\bar{g}_{\alpha\beta} = g_{\alpha\beta} - \frac{p_\alpha p_\beta}{M^2}, \quad \bar{\gamma}_\alpha = \gamma_\alpha - \frac{p_\alpha}{M^2} \not{p}. \tag{27}$$

- 
- [1] R. Bradford *et al.* [CLAS Collaboration], Phys. Rev. C **73**, 035202 (2006).
  - [2] K. Tsukada *et al.*, Phys. Rev. C **78**, 014001 (2008).
  - [3] T. Watanabe *et al.*, Phys. Lett. **B651**, 269-274 (2007).
  - [4] S. Janssen, J. Ryckebusch, D. Debruyne and T. Van Cauteren, Phys. Rev. C **65**, 015201 (2002).
  - [5] T. Mart, Phys. Rev. **C83**, 048203 (2011).
  - [6] B. G. Yu, T. K. Choi, W. Kim, Phys. Lett. **B701**, 332-335 (2011).
  - [7] L. De Cruz, D. G. Ireland, P. Vancraeyveld, J. Ryckebusch, Phys. Lett. **B694**, 33-37 (2010).
  - [8] T. Corthals, J. Ryckebusch and T. Van Cauteren, Phys. Rev. C **73**, 045207 (2006).
  - [9] T. Corthals, D. G. Ireland, T. Van Cauteren and J. Ryckebusch, Phys. Rev. C **75**, 045204 (2007).
  - [10] L. Guo and D. P. Weygand [CLAS Collaboration], arXiv:hep-ex/0601010.
  - [11] K. Hicks and W. Tang, AIP Conf. Proc. **1374**, 177 (2011).
  - [12] M. Nanova *et al.* [CBELSA/TAPS Collaboration], Eur. Phys. J. A **35**, 333 (2008).
  - [13] I. Hleiqawi and K. Hicks, arXiv:nucl-ex/0512039.
  - [14] I. Hleiqawi *et al.* [CLAS Collaboration], Phys. Rev. C **75**, 042201 (2007) [Erratum-ibid. C **76**, 039905 (2007)].
  - [15] S. H. Hwang *et al.* [CLAS Collaboration], Phys. Rev. Lett. **108**, 092001 (2012).
  - [16] Y. Oh and H. Kim, Phys. Rev. C **73**, 065202 (2006).
  - [17] Y. Oh and H. Kim, Phys. Rev. C **74**, 015208 (2006).
  - [18] S. Ozaki, H. Nagahiro and A. Hosaka, Phys. Rev. C **81**, 035206 (2010).
  - [19] S. H. Kim, S. i. Nam, Y. Oh and H.-Ch. Kim, Phys. Rev. D **84**, 114023 (2011).
  - [20] Q. Zhao, J. S. Al-Khalili and C. Bennhold, Phys. Rev. C **64**, 052201 (2001).
  - [21] K. Nakamura [Particle Data Group], J. Phys. G **37**, 075021 (2010).
  - [22] Y. Oh, C. M. Ko and K. Nakayama, Phys. Rev. C **77**, 045204 (2008).
  - [23] V. G. J. Stoks and T. A. Rijken, Phys. Rev. C **59**, 3009 (1999).
  - [24] S. Capstick, Phys. Rev. D **46**, 2864 (1992).
  - [25] S. Capstick and W. Roberts, Phys. Rev. D **58**, 074011 (1998).
  - [26] H. Haberzettl, C. Bennhold, T. Mart and T. Feuster, Phys. Rev. C **58**, 40 (1998).
  - [27] R. M. Davidson and R. Workman, Phys. Rev. C **63**, 025210 (2001).
  - [28] H. Haberzettl, K. Nakayama and S. Krewald, Phys. Rev. C **74**, 045202 (2006).
  - [29] D. Black, M. Harada and J. Schechter, Phys. Rev. Lett. **88**, 181603 (2002).
  - [30] W. Rarita and J. Schwinger, Phys. Rev. **60**, 61 (1941).
  - [31] B. J. Read, Nucl. Phys. B **52**, 565 (1973).
  - [32] R. Machleidt, K. Holinde and C. Elster, Phys. Rept. **149**, 1 (1987).
  - [33] V. V. Molchanov *et al.* [SELEX Collaboration], Phys. Lett. B **590**, 161 (2004) [hep-ex/0402026].
  - [34] R. H. Hackman, N. G. Deshpande, D. A. Dicus and V. L. Teplitz, Phys. Rev. D **18**, 2537 (1978).

- [35] J. W. Darewych, M. Horbatsch and R. Koniuk, Phys. Rev. D **28**, 1125 (1983).
- [36] C. L. Schat, C. Gobbi and N. N. Scoccola, Phys. Lett. B **356**, 1 (1995) [hep-ph/9506227].
- [37] A. Abada, H. Weigel and H. Reinhardt, Phys. Lett. B **366**, 26 (1996) [hep-ph/9509396].
- [38] G. Wagner, A. J. Buchmann and A. Faessler, Phys. Rev. C **58**, 1745 (1998) [nucl-th/9808005].
- [39] H. -Ch. Kim, M. Polyakov, M. Praszalowicz, G. -S. Yang and K. Goeke, Phys. Rev. D **71**, 094023 (2005) [hep-ph/0503237].
- [40] A. I. Titov and T. S. H. Lee, Phys. Rev. C **66**, 015204 (2002).
- [41] R. Bradford *et al.* [CLAS Collaboration], Phys. Rev. C **75**, 035205 (2007).
- [42] S. i. Nam, Phys. Rev. C **81**, 015201 (2010).